

See discussions, stats, and author profiles for this publication at: <https://www.researchgate.net/publication/231646972>

# Fischer–Tropsch Synthesis: Influence of Mn on the Carburization Rates and Activities of Fe-Based Catalysts by TPR–EXAFS/XANES and Catalyst Testing

ARTICLE *in* THE JOURNAL OF PHYSICAL CHEMISTRY C · FEBRUARY 2011

Impact Factor: 4.77 · DOI: 10.1021/jp111728h

---

CITATIONS

13

READS

61

## 7 AUTHORS, INCLUDING:



[Venkat Ramana Rao Pendyala](#)

University of Kentucky

52 PUBLICATIONS 372 CITATIONS

[SEE PROFILE](#)



[Burtron Davis](#)

University of Kentucky

605 PUBLICATIONS 11,042 CITATIONS

[SEE PROFILE](#)



[Donald C. Cronauer](#)

Argonne National Laboratory

122 PUBLICATIONS 1,234 CITATIONS

[SEE PROFILE](#)



[Arthur Jeremy Kropf](#)

Argonne National Laboratory

186 PUBLICATIONS 2,987 CITATIONS

[SEE PROFILE](#)

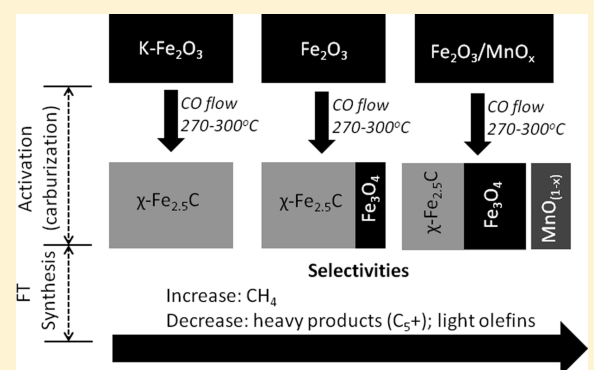
# Fischer–Tropsch Synthesis: Influence of Mn on the Carburization Rates and Activities of Fe-Based Catalysts by TPR-EXAFS/XANES and Catalyst Testing

Mauro C. Ribeiro,<sup>†</sup> Gary Jacobs,<sup>†</sup> Ramana Pendyala,<sup>†</sup> Burtron H. Davis,<sup>†,\*</sup> Donald C. Cronauer,<sup>‡</sup> A. Jeremy Kropf,<sup>‡</sup> and Christopher L. Marshall<sup>†</sup>

<sup>†</sup>Center for Applied Energy Research, University of Kentucky, 2540 Research Park Drive, Lexington, Kentucky 40511, United States; 1-859-257-0251;

<sup>‡</sup>Chemical Sciences and Engineering Division, Argonne National Laboratory, 9700 South Cass Avenue, CSE/205, Argonne, Illinois 60439-4837, United States

**ABSTRACT:** Fe-based catalysts containing different amounts of Mn were tested for Fischer–Tropsch synthesis using a stirred tank reactor at 270 °C, 1.21 MPa, and H<sub>2</sub>:CO = 0.7. Catalyst activation by carburization with 10% CO/He was followed by Temperature Programmed Reduction/X-ray Absorption Spectroscopy (TPR-EXAFS/XANES) from room temperature to 300 °C.  $\gamma$ -Fe<sub>2</sub>O<sub>3</sub> was converted into iron carbides, whereas MnO<sub>x</sub> was reduced to oxygen deficient MnO. Mn hindered Fe carburization, such that the carburized catalyst displayed higher Fe<sub>3</sub>O<sub>4</sub> content than the catalyst without Mn. EXAFS fitting indicates that the carburized catalyst contained a mixture of Hägg carbide, Fe<sub>3</sub>O<sub>4</sub>, and Mn oxides. Increasing Mn content led to higher CH<sub>4</sub> and light product selectivities, and lower light olefin selectivities. Higher and stable conversions were obtained with a catalyst containing an almost equimolar Fe/Mn ratio relative to the catalyst without Mn. Selectivity trends are attributed to the higher WGS rates observed on the FeMn catalysts, consistent with the structural differences observed.



## 1. INTRODUCTION

Fischer–Tropsch synthesis (FTS) is the catalytic hydrogenation of carbon monoxide to yield a mixture of hydrocarbons and oxygenates with molecular weights ranging from light gases (C<sub>1</sub>–C<sub>4</sub>) to heavy waxes (C<sub>30+</sub>). Small quantities of Cu, Si, and K are normally used as promoters in the Fe catalysts. The addition of Cu improves the reducibility of Fe oxides (e.g., Fe<sub>2</sub>O<sub>3</sub>, Fe<sub>3</sub>O<sub>4</sub>) during catalyst activation,<sup>1</sup> whereas the presence of Si increases the surface area of the active catalyst by stabilizing smaller particles. Potassium is known to facilitate carburization during catalyst activation and to enhance the selectivity for high molecular weight products.<sup>1,2</sup> Mn has also been studied, yet to a lesser extent, as a promoter, particularly after Kölbel et al. claimed in a patent<sup>3</sup> that higher selectivities for light products might be obtained over FeMn catalysts (with or without promotion by Cu and K). According to the authors, even if Fe is the minority component (the authors mention compositions with at least 50 wt.% Mn in their catalysts), high activities with high selectivities for the light olefins (C<sub>2</sub>–C<sub>4</sub>) were attained with low methane selectivity. Compared to Fe, Mn has a higher oxidation potential ( $\Delta E^{\circ}_{\text{Fe}^{2+}/\text{Fe}^0} = -0.447 \text{ V}$ ;  $\Delta E^{\circ}_{\text{Mn}^{2+}/\text{Mn}^0} = -1.185 \text{ V}$ )<sup>4</sup> and, therefore, its oxide is more stable, especially in the high partial pressures of steam found in FTS conditions. At the same conditions, Fe is known to be

present in the form of a heterogeneous mixture of magnetite (Fe<sub>3</sub>O<sub>4</sub>) and iron carbides.

Due to their comparable ionic radii, these two elements tend to form mixed oxides after air calcination, with a distribution of Fe and Mn ions in both tetrahedral and octahedral sites. Much research has been focused on determining how interactions between Fe and Mn phases in the working catalyst might promote the generation of light products at high conversion levels with reportedly no appreciable increase in CH<sub>4</sub> selectivity.

After Kölbel's patent, many studies also pointed to, although not without some disagreement,<sup>5</sup> confirmation that high selectivity for light olefins and low methane selectivity were obtained in coprecipitated FeMn catalysts activated with H<sub>2</sub>.<sup>6</sup> From those studies, the general picture that emerged then is that the H<sub>2</sub> activated catalyst is a mixture of (mixed) spinels Mn<sub>x</sub>Fe<sub>(3-x)</sub>O<sub>4</sub> and wustites (Fe,Mn)O, as well as metallic iron.<sup>7–10</sup> The metallic iron particles are considered to be partially covered by a Mn containing phase that decreases both CO and H<sub>2</sub> adsorption capacities.<sup>11–16</sup> These results were confirmed by more recent studies based on X-ray Near-Edge Absorption Spectroscopy (XANES) both with Fe<sup>17</sup> and Co.<sup>18,19</sup>

**Received:** December 9, 2010

**Revised:** January 20, 2011

**Published:** February 24, 2011

In addition, this mixed oxide phase tends to inhibit crystallite growth and thus, smaller Fe particles are retained.<sup>9,20,21</sup> Initially, the catalyst thus presents high activity and selectivity for light products with enhanced olefin-to-paraffin ratios. However, the structure of the catalyst changes as a function of reaction time, with the mixed oxide phase decomposing into iron carbides, magnetite, and MnO, thereby resulting in lower olefin selectivities.<sup>13,14,22</sup> In that case, MnO acts as a structural promoter because it can, even at high concentration, promote the activity by retaining a high surface area of Fe carbides.<sup>12</sup> Some authors have also claimed an increase in intrinsic activity as well.<sup>23,24</sup> The FeMn catalysts in these studies were typically activated with H<sub>2</sub>, and the focus was on a metallic Fe catalyst.

Higher activities are attained when the Fe catalyst is activated by carburization under CO flow.<sup>25</sup> Such treatment maximizes the formation of iron carbides, which are suggested to be the most important active phase for Fe-based FTS.<sup>25</sup> It is also the resulting active phase even after H<sub>2</sub>-reduced metallic Fe catalysts are exposed to FT conditions for a short length of time.

Therefore, in the present work, the carburization of Mn-doped Fe catalysts using CO was studied by *in situ* TPR-EXAFS/XANES at both the Fe and Mn K-edges. Carburized catalysts containing low (Fe:Mn 100:30) and high Mn (Fe:Mn 100:90) atomic ratios were tested for FTS using a continuously stirred tank reactor (CSTR). The results were compared to catalytic tests made with Mn-free Fe catalysts. The presence of Mn increases CO conversion on a per gram of Fe basis, as well as methane, light gas, and water-gas shift (WGS) selectivities. Such changes in the selectivities are correlated to the presence of different phases in the activated catalyst.

## 2. EXPERIMENTAL SECTION

**2.1. Catalyst Preparation.** In preparing the FeMn catalysts, the total metal concentration (Fe(III) + Mn(II)) in the feed liquid was kept at  $\sim 1.5 \text{ mol L}^{-1}$ . After dilution of the salts and addition of tetraethylorthosilicate (TEOS), the solution was stirred for 1 h until total dilution/hydrolysis of the TEOS had occurred. After that, the temperature was raised to  $80 \pm 5^\circ\text{C}$  and maintained for 100 min. Then, the Fe(III)/Mn(II) containing solution was pumped along with the ammonia solution ( $12 \text{ mol L}^{-1}$ ) into another beaker at twice the stoichiometric amount of NH<sub>3</sub> necessary to precipitate the Fe/Mn solids.

After final addition, the precipitate was digested under strong paddle stirring at  $75 \pm 5^\circ\text{C}$  for 1 h. The final precipitate was filtered and the remaining cake was washed twice in 1 L deionized water at  $60 \pm 10^\circ\text{C}$  for 30 min. The final solids were dried at  $120^\circ\text{C}$  for 24 h. After that, the catalyst precursor was calcined according to the following procedure:  $200^\circ\text{C}$  for 2 h and then  $350^\circ\text{C}$  for 5 h in a muffle furnace under static air atmosphere. Elemental analysis of the samples was carried out both at Galbraith Laboratories and in the CAER Analytical Laboratory, with good agreement between the results. Atomic and weight percentages of the samples are presented in Table 1.

**2.2. Catalyst Characterization.** **2.2.1. BET Surface Area and Porosity Measurements.** BET surface area and porosity (e.g., pore volume, average pore radius) measurements were performed on the calcined catalysts and results are summarized in Table 2. Before the BET experiment, the samples were degassed for 24 h at  $160^\circ\text{C}$  and 50 mTorr. All of the calcined catalysts presented similar surface areas and pore radii that were not measurably changed by impregnation with K.

**Table 1. N<sub>2</sub> Adsorption Analysis Results<sup>a</sup>**

sample	atomic composition (in the solution) <sup>a</sup>	atomic composition (in the catalyst precursor)
Fe	100Fe:5.1Si	100Fe:5.1Si
FeK	100Fe:5.1Si:3K	100Fe:5.1Si:3K
100Fe5Mn	100Fe:5.1Si:5Mn	100Fe:5.1Si:5.5Mn
100Fe15Mn	100Fe:5.1Si:15Mn	100Fe:5.1Si:16.5Mn
100Fe30	100Fe:5.1Si:30Mn	100Fe:5.1Si:33.2Mn
100Fe5Mn3	100Fe:5.1Si:5Mn:3K	100Fe:5.1Si:5.5Mn:3K
100Fe30Mn3K	100Fe:5.1Si:30Mn:3K	100Fe:5.1Si:33.2Mn:3K
100Fe90Mn3K	100Fe:120Mn:5.1Si	100Fe:90.1Mn:5.5Si:3K

<sup>a</sup> K was added afterward as a KNO<sub>3</sub> solution, by impregnation.

**Table 2. Atomic and Weight Percent of the Catalysts Used in This Work<sup>a</sup>**

composition	BET S.A. (cm <sup>2</sup> g <sup>-1</sup> )	adsorption pore volume (cm <sup>3</sup> g <sup>-1</sup> )	adsorption pore radius (nm)
100Fe:5.1Si	183.8	0.32	2.8
100Fe:5.1Si:3K	184.0	0.29	2.6
100Fe:5.1Si:5Mn	199.9	0.34	2.7
100Fe:5.1Si:5Mn:3K	178.1	0.31	2.8
100Fe:5.1Si:15Mn	206.6	0.36	2.8
100Fe:5.1Si:15Mn:3K	189.1	0.32	2.8
100Fe:5.1Si:30Mn	201.4	0.36	2.9
100Fe:5.1Si:30Mn:3K	202.2	0.36	2.9
100Fe:5.1Si:90Mn:3K	163.6	0.23	2.4

<sup>a</sup> Catalyst precursors calcined at  $350^\circ\text{C}$  for 5 h in static atmosphere.

**2.2.2. TPR-EXAFS/XANES.** Activation of the FeMn catalysts under CO/He flow was investigated by XAS at both the Fe and Mn K-edges (7.112 and 6.539 keV, respectively). The temperature was increased for 7 h from room temperature to  $300^\circ\text{C}$  and then held constant at that temperature for 5 h. Successive X-ray absorption spectra were recorded during sample carburization.

XAS spectra were treated using the WinXAS<sup>26</sup> software. After being background subtracted, the spectra (in energy space) were trimmed above 7.65 keV (Fe K-edge) and 7.04 keV (Mn K-edge). The spectra were then normalized with a Victoreen function and further normalized with a two-polynomial function of degree 1 for the pre- and postedge regions. XANES spectra were then obtained by sectioning the baseline-corrected spectra from 7.07 to 7.202 keV (Fe K-edge) and 6.53 to 6.64 keV (Mn K-edge).

After background removal and normalization, the spectra were converted to k-space and background subtracted in k-space using a cubic spline fit. The spectra were then truncated within the range of 2.0 to 10.3 (Fe K-edge) and 2.0 to 11.1 Å<sup>-1</sup> (Mn K-edge). To obtain the phase uncorrected radial distribution function, the Fourier transform was carried out, making use of a Bessel window function; a k-weighting of 3 was employed, to emphasize scattering by the heavy atoms (i.e., Fe and Mn).<sup>27</sup>

**2.3. Catalytic Testing Using a CSTR.** For catalytic testing, a 1 L continuously stirred tank reactor (CSTR) was used in this study. The calcined catalyst precursors were activated by *in situ* carburization under CO flow for 24 h at  $270^\circ\text{C}$  and 1.21 MPa. During carburization, the temperature was ramped from room temperature to  $150^\circ\text{C}$  in 2 h under N<sub>2</sub> and then from 150 to  $270^\circ\text{C}$  in 2 h under CO flow ( $3 \text{ sLh}^{-1} \text{ g}_{\text{Fe}}^{-1}$ ). After activation

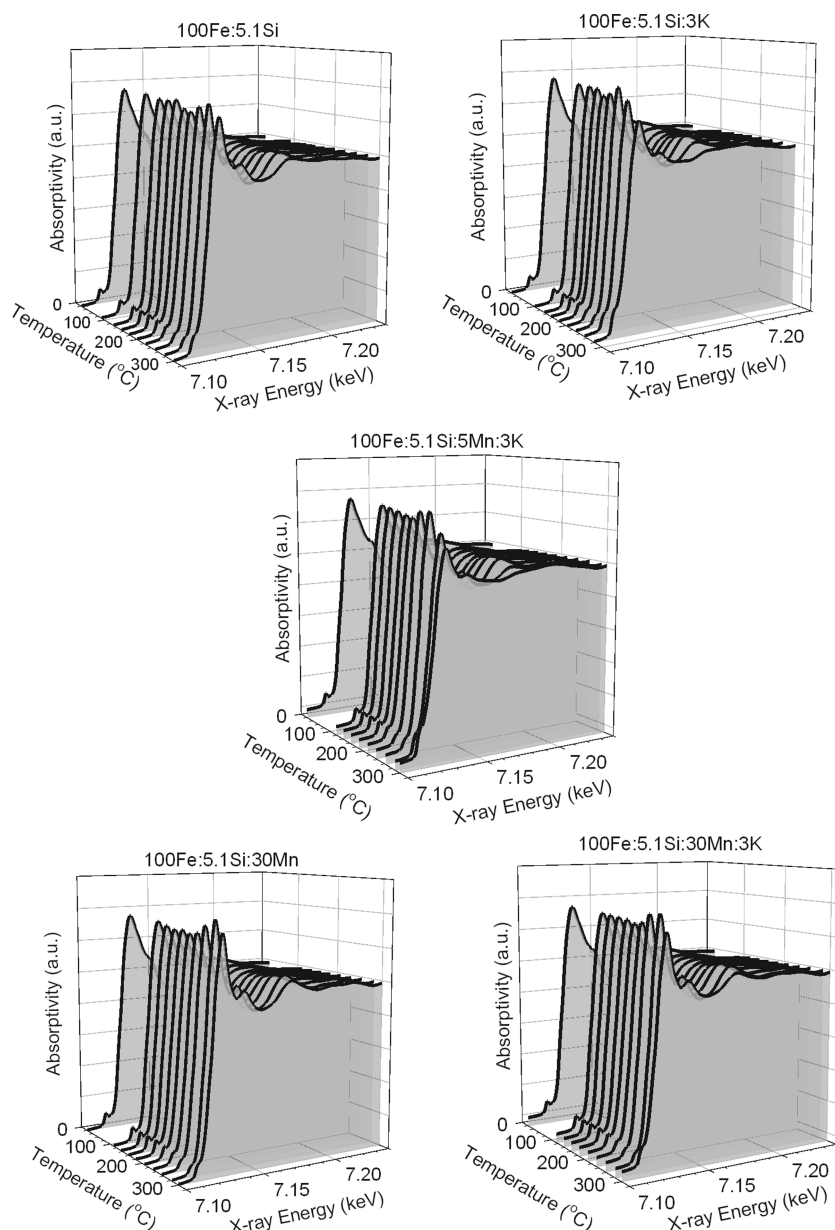


**Figure 1.** Fe K-edge TPR-XANES of the FeMn samples.

in CO, the reactor was fed with syngas ( $\text{H}_2:\text{CO} = 0.7$ ) at a space velocity of  $7 \text{ sLh}^{-1} \text{ g}_{\text{Fe}}^{-1}$  (standard conditions:  $T = 273.15 \text{ K}$ ,  $P = 760 \text{ mm Hg}$ ,  $270 \text{ }^{\circ}\text{C}$ ). Removal of the wax samples from the catalyst slurry was performed using a sintered metal filter that was installed in the reactor. The wax sample was extracted through the internal filter and collected in a hot trap held at  $200 \text{ }^{\circ}\text{C}$ . A warm trap ( $100 \text{ }^{\circ}\text{C}$ ) and cold trap ( $0 \text{ }^{\circ}\text{C}$ ) were used to collect light wax and the water plus oil samples, respectively, by condensing them from the vapor phase that was continuously withdrawn from the reactor vapor space. On a daily basis, gas, water, oil, light, and heavy wax samples were collected and analyzed. The tail gas from the cold trap was analyzed with an online HP Quad Series Micro GC, providing molar compositions of  $\text{C}_1\text{--C}_7$  olefins and paraffins as well as for  $\text{H}_2$ ,  $\text{CO}$ , and  $\text{CO}_2$ . Hydrogen and carbon monoxide conversions were calculated based on the gas product GC analysis results and the gas flow measured at the reactor outlet. The oil and light wax samples were mixed

and separated from the water layer before analysis with an Agilent 6890 Series GC. The heavy wax was analyzed with an HP5890 Series II Plus high temperature GC, while the water sample was analyzed using an HP5790 GC.

### 3. RESULTS AND DISCUSSION

**3.1. TPR-XANES.** In order to investigate the effect of Mn on catalyst activation in CO, the samples were studied by TPR-XANES. Figure 1 shows the evolution of the Fe K-edge XANES spectra as the temperature was increased from 25 to  $300 \text{ }^{\circ}\text{C}$ . Closer inspection of the Fe K-edge XANES spectra in Figure 1 shows that: (a) spectra taken at temperatures below  $200 \text{ }^{\circ}\text{C}$  present small preedge peaks and (b) there is a variation in the white line intensities as the carburization temperature was increased. The dried product from the precipitation of Fe(III) with ammonia solution is composed of a complex mixture of Fe

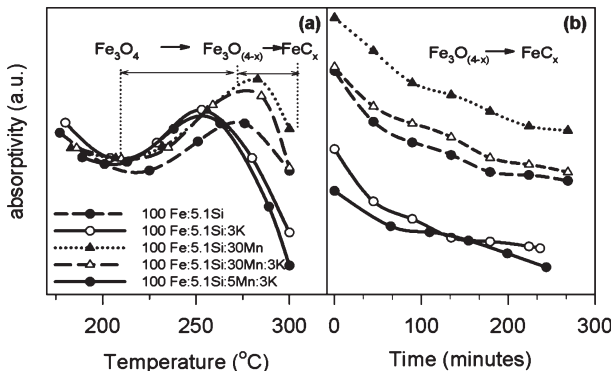


**Figure 2.** Fe K-edge TPR-XANES white line maxima as a function of carburization temperature (a) and time at 300 °C (b).

oxyhydroxides ( $\text{FeOOH}$ )<sup>20</sup> that after calcination at 350 °C gives hematite ( $\text{Fe}_2\text{O}_3$ ), which occurs in two possible phases:  $\alpha$  and  $\gamma$ - $\text{Fe}_2\text{O}_3$ . The  $\text{O}^{2-}$  ions in  $\alpha$ - $\text{Fe}_2\text{O}_3$  are present in a hexagonal arrangement, with Fe(III) ions occupying exclusively octahedral sites.  $\gamma$ - $\text{Fe}_2\text{O}_3$  has a cubic arrangement of  $\text{O}^{2-}$  ions with Fe(III) occupying randomly both octahedral and tetrahedral sites.<sup>28</sup> In the XANES spectra, the presence of pre-edge peak structures is related to the symmetry of the sites occupied by the absorber. The higher the symmetry, the lower the intensity of the pre-edge peak will be.<sup>29</sup> Therefore, very low intensity pre-edge structures, if any, would be expected for transition metals located in octahedral sites, whereas more intense pre-edge peaks are observed in ions located in less symmetric, tetrahedral sites. Therefore, the presence of small pre-edge peaks in the XANES spectrum taken at room temperature (Figure 1) suggests that the iron phase in our calcined material might be  $\gamma$ - $\text{Fe}_2\text{O}_3$  or at least a mixture of  $\alpha$  and  $\gamma$ - $\text{Fe}_2\text{O}_3$ . The presence of a mixed  $\text{Fe}_{2-x}\text{Mn}_x\text{O}_3$  oxide phase cannot be ruled out, and has been suggested to exist by others.<sup>7–10</sup> Nevertheless, in examining the Fe K-edge results, although we observed differences in rates of carburization between catalyst samples with and without Mn, we did not detect discernible line shape differences in the XANES spectra between the intermediary iron oxides along the TPR trajectory. Moreover, in fitting the EXAFS results of carburized samples with and without Mn, acceptable fittings were obtained by considering only  $\text{Fe}_3\text{O}_4$  and Hägg carbide. In the future, it may be instructive to carry out TPR-XAS and XRD over more crystalline samples to try to pinpoint a mixed oxide phase. The samples used in our work are limited to short-range order.

The differences among white line peak intensity profiles as a function of temperature (Figure 1) are better illustrated in Figure 2, where the dependence of the maximum in the white line absorptivity with temperature during the temperature increase up to 300 °C (Figure 2a), as well as during the 5 h temperature hold at 300 °C, are presented. This variation in the white line intensities with carburization temperature has been ascribed to the stepwise reduction of  $\text{Fe}_2\text{O}_3$  to  $\text{Fe}_3\text{O}_4$  and then to  $\text{FeC}_x$ .<sup>1,2</sup> This last transition is suggested to take place involving an oxygen deficient form of  $\text{Fe}_3\text{O}_4$  (which we refer to here as  $\text{Fe}_3\text{O}_{(4-x)}$ ),<sup>30</sup> such that the white line intensity first increases to a maximum (i.e., O-deficient  $\text{Fe}_3\text{O}_4$ ), and then decreases at temperatures above 280 °C, as iron carbides are formed. From Figure 2a it can be seen that this reduction process is influenced by both K and Mn. Further insight into the carburization process was obtained by observing the carburization process at 300 °C for

nearly 3 h, with Figure 2b depicting the dependence of the white line peak intensities in Fe K-edge spectra with carburization time at 300 °C. As a general picture, samples containing Mn underwent slower carburization of Fe, indicating that Mn hinders the Fe carburization rate. The presence of K increased the carburization rates, as expected from our previous observations.<sup>1,2</sup> White line intensities obtained from the carburization of the 100Fe5.1Si5Mn3K sample were similar to the 100Fe5.1Si3K sample, suggesting that the presence of such small quantities of Mn does not influence the carburization process significantly.

Figure 3 shows the evolution of Mn K-edge XANES as a function of temperature. In all the samples,  $\text{MnO}_x$  is progressively reduced giving rise to different XANES spectra as the carburization temperature was increased. Mn compound reference spectra were taken from NSLS's X18-X19 database.<sup>31</sup> In Figure 4, the absorption edge structures of the spectra taken at energies near the Mn K-edge, as a function of the carburization temperature, are presented.

The absorption edge of the Mn in the calcined samples before carburization (spectra at 21 °C in Figure 4a–c) is similar to that of the  $\text{Mn}_2\text{O}_3$  reference, with the difference being that the white line is more intense than in the reference, probably due to a change in the density of available states near the Fermi level caused by the presence of small particles.<sup>32</sup> Nevertheless, the similarity of the edge energy of the spectra of the calcined catalyst to the  $\text{Mn}_2\text{O}_3$  reference spectra implies that Mn in the calcined samples is in an oxidation state of III. The shift of the absorption edge (given by the inflection points shown in Figure 4a) toward energies closer to the  $\text{Mn}^0$  edge (6.539 keV) as the carburization temperature increases shows that Mn is further reduced during sample carburization. The fact that in all samples the Mn absorption edge occurs at energies between the metallic Mn and the  $\text{MnO}$  reference suggests that Mn is present in the catalyst carburized at 300 °C as a form of oxygen-deficient  $\text{MnO}$ , probably in the same way  $\text{TiO}_2$  in the metal oxide interface is present in the form of a partially reduced oxide, in Pt-TiO<sub>2</sub> catalysts.<sup>33</sup> The presence of Fe(II) in this  $\text{MnO}_x$  phase cannot be ruled out, although a definitive characterization by analysis of the XANES results is challenging. The same is true regarding the presence of manganese carbides. However, there has not been reported any evidence of formation of a manganese carbide phase in previous studies, and its stability under Fischer–Tropsch synthesis conditions, in which  $\text{H}_2\text{O}$  is a major product, is doubtful. Figure 4b shows that Mn oxide in sample 100Fe5Mn3K was reduced to the O-deficient  $\text{MnO}$  form at lower temperatures than in the other samples containing higher Mn contents. If one considers that as the FeMn sample is carburized at increasingly higher temperatures and Mn segregates as small particles of  $\text{MnO}_x$  binding Fe containing species (in the form of  $\text{Fe}_3\text{O}_4$  or  $\text{FeC}_x$ ), the  $\text{MnO}_x$  that is in direct contact with Fe (*interfacial*  $\text{MnO}_x$ ) might be more easily reduced than the  $\text{MnO}_x$  that is in the bulk of the particle, probably due to the spillover of CO from carburized Fe centers at the interfacial boundary to  $\text{MnO}_x$ , in the same manner as  $\text{H}_2$  dissociation and spillover is suggested to be involved in the activation of noble metal promoted cobalt FT catalysts.<sup>34</sup> Hence, since with the lower Mn content sample, the ratio between the *interfacial*  $\text{MnO}_x$  and the *bulk*  $\text{MnO}_x$  is higher than in the more Mn rich samples, the overall  $\text{MnO}_x$  reduction rate will likewise be higher.

Closer inspection of Figure 4b reveals that the reduction of  $\text{MnO}_x$  species occurs at somewhat lower temperatures in the 100Fe30Mn3K sample than in 100Fe30Mn, suggesting that the

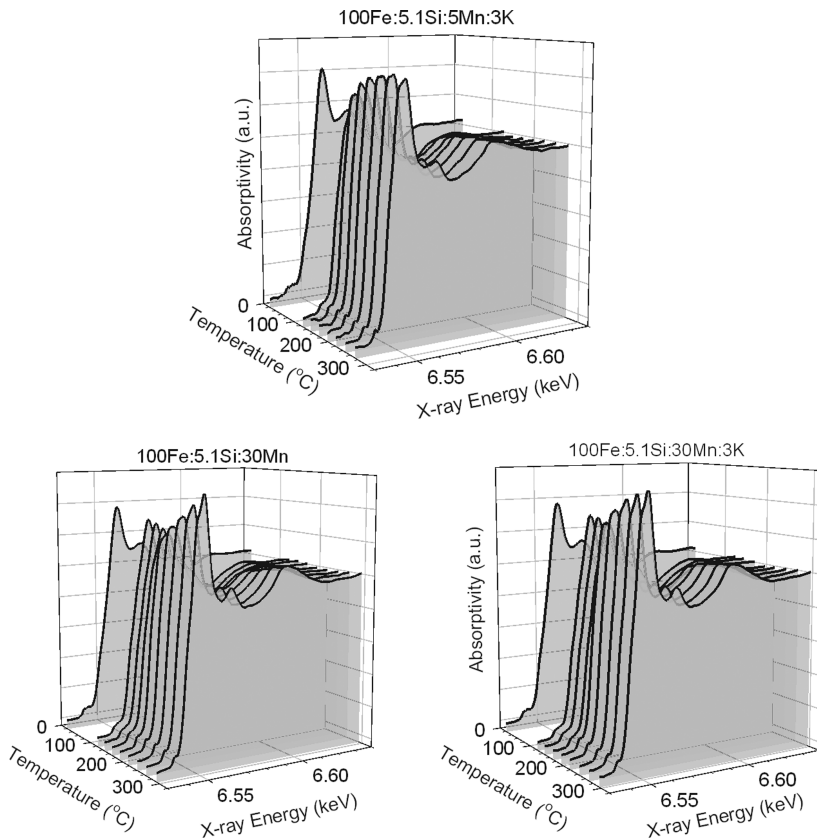


**Figure 3.** Mn K-edge TPR-XANES of the FeMn samples.

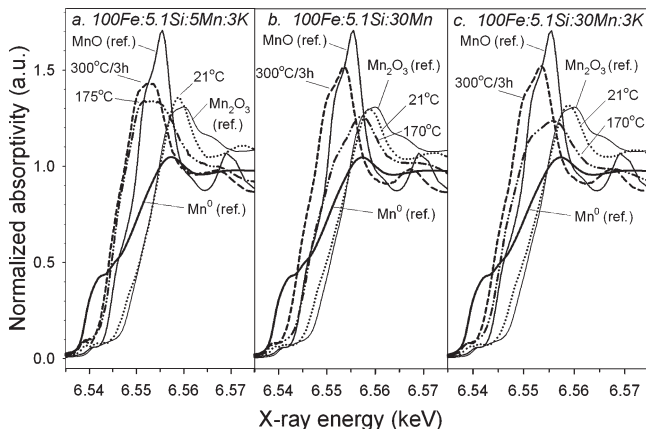


**Figure 4.** Mn K-edge XANES spectra at different carburization temperature of different FeMnSiK samples, in comparison with references for Mn<sub>2</sub>O<sub>3</sub>, MnO, and Mn<sup>0</sup>.

presence of K facilitates reduction of Mn oxides, probably by an increase in the surface reactivity toward the dissociative adsorption of CO.<sup>2</sup>

**3.2. TPR-EXAFS.** Figure 5 shows the  $k^3$  weighted Fourier transform magnitude spectra of the different Fe catalyst samples used in the study both during the temperature ramp up to 300 °C (Figure 5a) and during the temperature hold at 300 °C for nearly 5 h (Figure 5b). At lower temperatures, there are two major peaks located between 1 and 2 Å and between 2 and 3 Å, respectively, corresponding to the Fe–O distance in the first Fe–O coordination shell around Fe ( $d = 1.9 - 2.1 \text{ \AA}$ ). The

second peak includes scattering by Fe atoms located in the first Fe–Fe coordination shell of Fe<sub>2</sub>O<sub>3</sub> (2.9 – 3.5 Å). As the temperature increased, the first peak (located between 1 and 2 Å) decreased its intensity, denoting reduction of Fe<sub>2</sub>O<sub>3</sub> to Fe<sub>3</sub>O<sub>4</sub>, with an expected decrease in the peak for Fe–O in the first coordination shell. The increase in the temperature results in a decrease in Fourier transform peak intensities, in part due to an increasing contribution from the Debye–Waller factor. However, considering the corresponding changes in the XANES data, the decrease is also due to reduction of Fe and the subsequent rearrangement of coordination shells around Fe centers. The evolution of the Fourier transform of the spectra taken at the 300 °C hold for ~5 h shows that in all samples, peaks for Fe–O and Fe–Fe coordination in Fe<sub>3</sub>O<sub>4</sub> decreased and a new peak formed at ~2 Å, corresponding to Fe–Fe coordination in Fe-carbides. Eventually, as can be seen in Figure 5b, a significant contribution from peaks characteristic of Fe–O and Fe–Fe coordination in Fe<sub>3</sub>O<sub>4</sub> for the unpromoted catalyst sample (100Fe:5.1Si) and the heavily Mn promoted samples remained, suggesting that much of the Fe is still in the oxide form even after the carburization treatment, whereas in the 100Fe:5.1Si:3K and 100:Fe5.1Si:5Mn:3K sample, the presence of only one large peak after nearly 5 h carburization at 300 °C suggests that essentially all the Fe is in the form of carbides. These results are in good agreement with the observation from TPR-XANES analysis, confirming that Mn hinders the Fe carburization process.

Iron is suggested to be present under typical FTS conditions as a mixture of magnetite and iron carbides.<sup>25</sup> Among the possible carbides, the ones that may occur under FTS conditions are the metastable  $\varepsilon$ -Fe<sub>2.2</sub>C, the  $\chi$ -Fe<sub>2.5</sub>C (Hägg carbide) and  $\theta$ -Fe<sub>3</sub>C

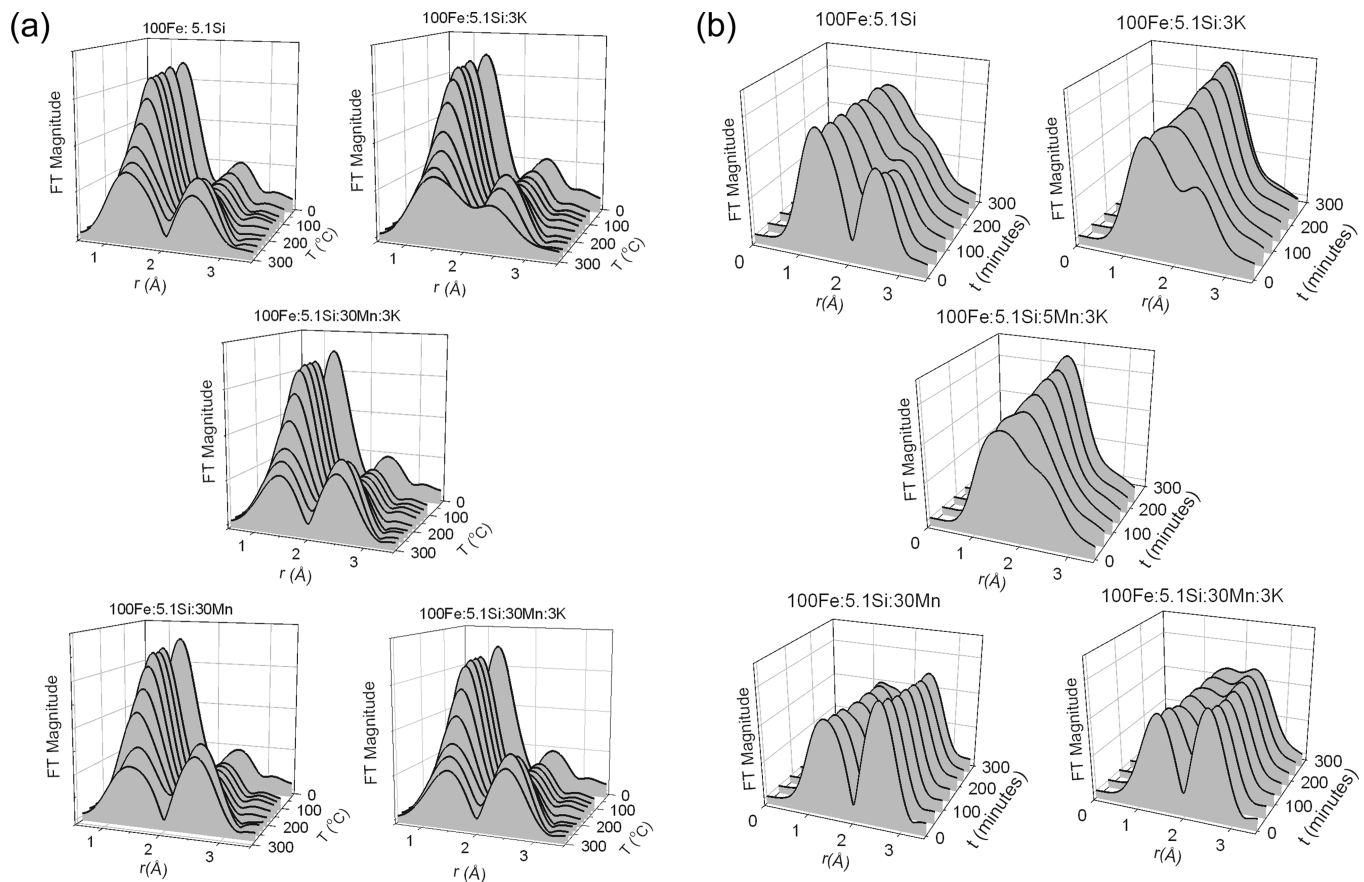


**Figure 5.** Fe K-edge  $k^{-3}$  weighted radial distribution functions of the spectra taken from the catalyst samples carburized during the temperature ramp (a) and at 300 °C for 5 h (b).

**Table 3. Results of EXAFS Fittings for Final Catalyst at 290 °C in Flowing CO/He<sup>a</sup>**

	phase	$\alpha$	A	Q (%) <sup>b</sup>	$\sigma^2$ (Å <sup>2</sup> )	$e_0$ (eV)	r-factor
100Fe:5.1Si	Hägg	-0.0448 (0.00577)	0.688 (0.104)	42	0.0134 (0.00175)	-15.62 (2.02)	0.019
	Fe <sub>3</sub> O <sub>4</sub>	0.00328 (0.00962)	0.286 (0.0596)			-8.43 (3.02)	
100Fe:5.1Si:3K	Hägg	-0.0448 (0.00577)	0.855 (0.116)	28	0.0134 (0.00175)	-15.32 (1.82)	
	Fe <sub>3</sub> O <sub>4</sub>	0.00328 (0.00962)	0.241 (0.0616)			-13.95 (3.21)	
100Fe:5.1Si:30Mn	Hägg	-0.0448 (0.00577)	0.561 (0.0871)	86	0.0134 (0.00175)	-16.16 (2.15)	
	Fe <sub>3</sub> O <sub>4</sub>	0.00328 (0.00962)	0.485 (0.0657)			-11.32 (2.67)	
100Fe:5.1Si:30Mn:3K	Hägg	-0.0448 (0.00577)	0.656 (0.0966)	64	0.0134 (0.00175)	-15.83 (2.01)	
	Fe <sub>3</sub> O <sub>4</sub>	0.00328 (0.00962)	0.418 (0.0654)			-12.19 (2.75)	
100Fe:5.1Si:5Mn:3K	Hägg	-0.0448 (0.00577)	0.863 (0.119)	60.5	0.0134 (0.00175)	-14.94 (1.83)	
	Fe <sub>3</sub> O <sub>4</sub>	0.00328 (0.00962)	0.253 (0.0644)			-13.59 (3.19)	

<sup>a</sup> Model considers the presence of Hägg carbide and Fe<sub>3</sub>O<sub>4</sub>. Fitting intervals:  $2.5 \text{ Å}^{-1} < k < 10.0 \text{ Å}^{-1}$ ;  $1.0 \text{ Å} < R < 3.0 \text{ Å}$ . Note that  $S_0^2$  was fixed at 0.9. Global parameters (i.e., over all samples) were used for the isotropic lattice expansion ( $\alpha$ ) for Hägg carbide and Fe<sub>3</sub>O<sub>4</sub> fractions; furthermore, a single global Debye–Waller factor ( $\sigma^2$ ) parameter was used. Local parameters (i.e., for each sample) were applied to the energy shift ( $e_0$ ) and amplitude function multipliers (A) of each component. <sup>b</sup> Percentage ratio between Fe<sub>3</sub>O<sub>4</sub> and Hägg carbide amplitude factors.

(cementite) forms.<sup>35</sup> Epsilon carbide is typically formed at lower temperatures (<250 °C), while the Hägg carbide is formed between 250 and 350 °C; cementite is formed at temperatures above 350 °C.<sup>35,36</sup> In order to determine the relative quantities of iron carbides and iron oxides in our 5 h/300 °C carburized catalysts, as a function of the presence of Mn and K promoters, fitting of the Fe-edge EXAFS spectra was performed.

In our fittings, only the presence of Hägg carbide was considered, partly because the carburization was performed at

a temperature where this type of carbide was expected to be in the majority<sup>33</sup> and partly because we could successfully fit EXAFS data of similar catalysts in our previous investigation of the impact of alkali promoters on Fe carburization.<sup>2</sup> Magnetite was considered to be the oxide phase present after carburization at 300 °C.<sup>25</sup> Single scattering paths up to 3.5 Å from the absorber were considered in the first shell fitting model. Table 3 shows the results of the fittings. An amplitude factor was assigned to each scattering path. This factor was dependent on the average

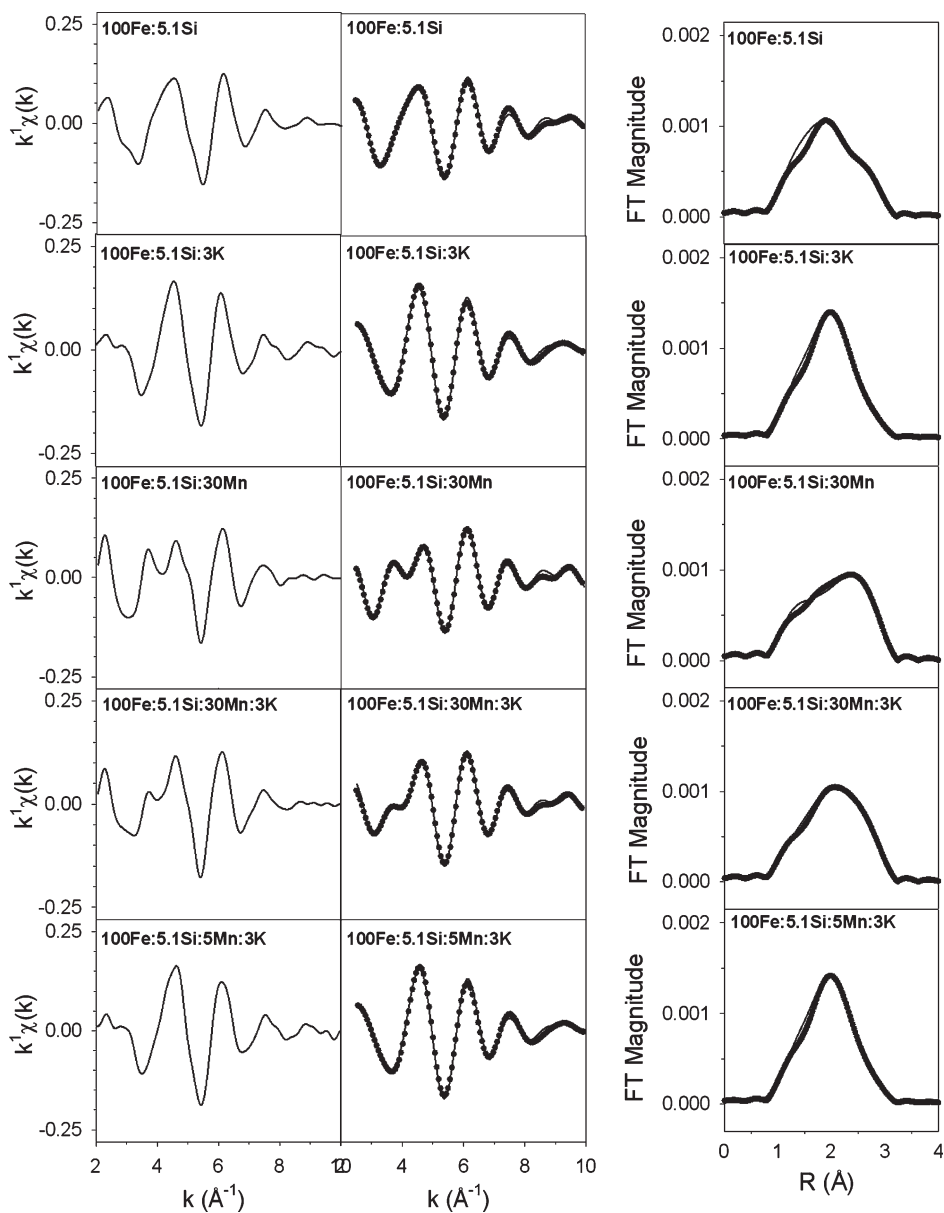


**Figure 6.** Results of EXAFS fittings for final catalyst at 290 °C in flowing CO/He (Fe K-edge,  $k^1$  weighed radial distribution functions). Model considers the presence of Hägg carbide and  $\text{Fe}_3\text{O}_4$ . Fitting intervals:  $2.5 \text{ \AA}^{-1} < k < 10.0 \text{ \AA}^{-1}$ ;  $1.0 \text{ \AA} < R < 3.0 \text{ \AA}$ . Note that  $S_0^2$  was fixed at 0.9. Global parameters (i.e., over all samples) were used for the isotropic lattice expansion ( $\alpha$ ) for Hägg carbide and  $\text{Fe}_3\text{O}_4$  fractions; furthermore, a single global Debye–Waller factor ( $\sigma^2$ ) parameter was used. Local parameters (i.e., for each sample) were applied to the energy shift ( $e_0$ ) and amplitude function multipliers ( $A$ ) of each component.

coordination number around the absorber due to both crystallite size and relative composition. We have fitted the spectra from all the samples using as common parameters a global expansion coefficient  $\alpha$  and a Debye–Waller factor  $\sigma^2$ . The former parameter was the lattice expansion parameter, and was the change in distance from the nominal bond length (e.g., negative values represent a contraction of the lattice). The latter parameter,  $\sigma^2$ , was related to the vibration of atoms around their equilibrium position.<sup>37</sup> Reasonable values for the global parameters ( $\alpha$ ,  $\sigma^2$ ) were obtained (Table 3), and the relatively low  $r$ -factor (i.e., goodness of fit parameter) indicates good agreement between the experimental data and the theoretical model, as shown in Figure 6. If the particle size (related to the average coordination number around the absorber) is similar for all the samples, then one may make inferences regarding the relative composition of

the carbide (Hägg) and oxide ( $\text{Fe}_3\text{O}_4$ ) by comparing the relative contributions ( $Q$ ) of the carbide and oxide phase to the amplitude function. The presence of potassium led to a promotion of the carburization rate, as can be seen by the larger  $Q$  value in comparison to that of the unpromoted catalyst. This trend was expected for Fe carburization when promoted by the presence of alkali, due to an increase in the CO dissociation rate.<sup>2</sup> Addition of Mn, however, lead to lower values of  $Q$ , and indicated, in agreement with the XANES results, that Mn hindered the carburization of Fe. Note that adding K to the Mn promoted catalysts did improve the carburization rate somewhat (i.e., higher  $Q$  values are observed) relative to the samples lacking K.

**3.3. FT testing.** Figure 7 depicts the results of reactor testing. The baseline comparison is made with a catalyst containing a small quantity of Cu. The catalysts present comparable CO

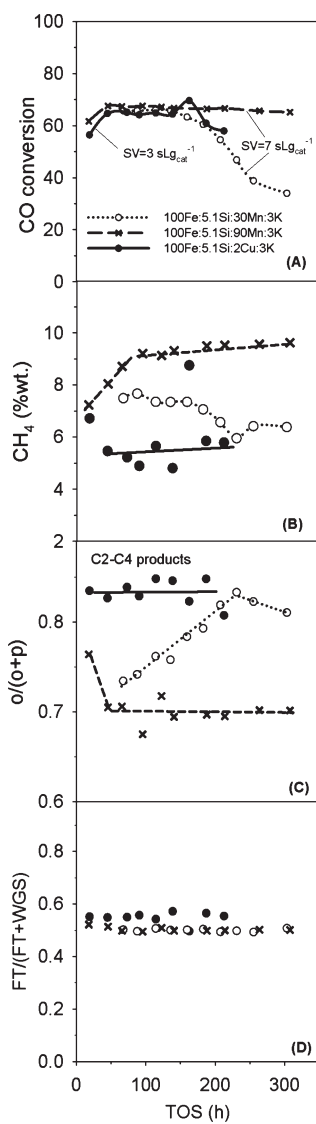


**Figure 7.** Reaction testing results in function of time on stream for 100Fe:5.1Si:30Mn:3K, 100Fe:5.1Si:90Mn:3K, and 100Fe:5.1Si:2Cu:3K. CO conversion (a); methane selectivity (b); olefin fraction (c); and FT to WGS fraction (d) as a function of time on stream. Testing conditions: 1.21 MPa, 270 °C, H<sub>2</sub>/CO ratio 0.7.

conversion levels (Figure 7a). Cu is known to enhance the reducibility of iron and therefore, enhance the active surface area.<sup>1,38</sup> Considering this and the fact that the Mn containing catalysts were tested at a considerably higher space velocity compared to a catalyst without Mn leads to the conclusion that the Mn containing catalysts were highly active. After 150 h, the 100Fe:5.1Si:30Mn:3K catalyst deactivated, with the CO conversion dropping from 65% to 40% over 150 h, unlike the 100Fe:5.1Si:90Mn:3K catalyst which maintained a steady CO conversion level during the entire test. The higher activity of the Mn containing catalyst can be explained by MnO stabilizing smaller Fe particles.

The selectivities, which are defined here as the number of moles of C going to the product of interest divided by the number of moles of CO converted, are shown in Figure 7b–d. The 100Fe:5.1Si:2Cu:3K catalyst shows a steady methane selectivity of around 5 wt %. As for the FeMn catalysts, methane

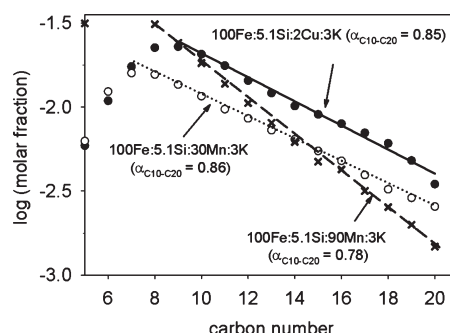


**Figure 8.**  $\alpha$ -Plots ( $C_{10} - C_{20}$ ) from the liquid products obtained in the tests. Testing conditions: 175 psi, 270 °C, H<sub>2</sub>/CO ratio 0.7. CO conversions around 65%; times on stream around 140 h.

selectivity is higher for the catalysts containing a higher quantity of Mn in the sample; furthermore, it changes with time on stream. Considering the 100Fe:5.1Si:30Mn:3K, it is difficult to conclude anything from the methane selectivity dependence on time on stream, as this parameter changes with the conversion level. However, the 100Fe:5.1Si:90Mn:3K sample, which presents steady conversion around 65%, shows an initial increase in the methane selectivity from 7 to 9 wt % and then approaches an almost steady value around 9%wt. This change indicates that the catalyst surface experienced important structural changes over the first 80 h of reaction.

Figure 7c shows the olefin fraction in the  $C_2 - C_4$  products. In contrast to previous reports of Mn-doped metallic iron catalysts, increasing quantities of Mn in the iron carbide catalyst led to a decrease in the olefin selectivity. As has been already mentioned, in the majority of literature studies of FeMn catalysts, the activation was carried out under H<sub>2</sub>, leading to the metallic iron state. Some authors noticed that olefin selectivity decreased with time on stream with the catalyst, whereby a mixture of metallic iron and a Fe<sub>x</sub>Mn mixed oxide phase was transformed into separate iron carbide and MnO phases.<sup>22</sup> It is already known that metallic iron suffers carburization under exposure to syngas.<sup>13,14,25,39</sup> It is possible then that any interaction between Fe and MnO supposedly present in the H<sub>2</sub> reduced catalyst and reportedly active for the olefin selectivity is lost when the Fe phase is carburized, as was the case for our samples that were treated in situ under CO flow at 270 °C for 24 h.

The ratio between the FT and WGS activities, depicted in Figure 7d (considered here to be the ratio between the number of moles of CO molecules converted to Fischer-Tropsch synthesis products over the total number of CO molecules consumed, per unit time) is lower in the FeMn catalysts than the 100Fe:5.1Si:2Cu:3K reference catalyst, which suggests that the presence of Mn generates active sites for WGS.

Figure 8 depicts the semilogarithmic plots for the molar fraction of FT products between  $C_{10}$  and  $C_{20}$  from liquid samples taken at CO conversions around 65% and times on stream around 140 h. The slope of these curves gives the chain growth probabilities ( $\alpha$ ) that may assume values between 0 and 1; the higher the chain growth probability the heavier the products that are obtained.<sup>40</sup> The presence of 30% Mn (relative to Fe) did not seem to influence chain growth probability in that chain length range, in comparison with the non-Mn containing catalyst, as both catalysts exhibited similar  $\alpha$ -values ( $\alpha(100Fe:5.1Si:30Mn:3K) = 0.86$ ;  $\alpha(100Fe:5.1Si:2Cu:3K) = 0.85$ ). However, 90% Mn caused a considerable decrease of the  $\alpha$ -value ( $\alpha = 0.78$ ),

denoting that the presence of a high Mn loading in the catalyst leads to a decrease in the selectivity for higher molecular weight products.

## 4. CONCLUSIONS

Catalysts with a general atomic composition 100Fe:5.1Si: $x$ Mn:3K have been tested for FTS in a CSTR. The effect of the carburization on the catalyst structure was examined by TPR-XANES/EXAFS. Following carburization at 300 °C, TPR/XANES analysis suggested that Mn is present as an oxygen deficient form of MnO. Good EXAFS fittings of the Fe K-edge spectra taken for the 3 h/300 °C carburized catalysts were obtained when  $\chi$ -Fe<sub>2.5</sub>C (Hägg carbide) and Fe<sub>3</sub>O<sub>4</sub> were considered in the model. The presence of Mn led to an increase in the catalyst activity, probably because it stabilized a higher dispersion of iron carbide particles. FTS on the carburized FeMn catalysts was accompanied by higher CH<sub>4</sub> and WGS selectivities—the two most likely being interrelated—as well as lower chain growth probability and lower olefin selectivity. The selectivity results reported herein are in contrast to the lower CH<sub>4</sub> and higher olefin selectivities observed over H<sub>2</sub> activated FeMn catalysts reported in the literature.<sup>9,17,18</sup> This suggests that the different structures obtained according to the activation treatment (H<sub>2</sub> reduction, which favors the metal versus carburization, which favors iron carbides) exhibit somewhat different catalytic properties. However, it should be emphasized that even if the catalyst is activated under H<sub>2</sub> prior to FTS, the lower CH<sub>4</sub> selectivity, as well as the higher olefin selectivity observed in the literature tend to be lost as a function of time onstream, as the Fe<sup>0</sup>/MnO, which is reportedly responsible for this behavior, converts to  $\chi$ -Fe<sub>2.5</sub>C/Fe<sub>3</sub>O<sub>4</sub>/MnO<sub>(1-x)</sub> carbide during FTS.<sup>13,14,19</sup> Thus, the current investigation tends to confirm that iron carbides lead to an increased CH<sub>4</sub> and light paraffin selectivity relative over the metal—probably due to enhanced WGS activity. Therefore, considering that metallic Fe catalysts convert to iron carbides with time onstream, there appears to be little benefit in adding Mn as a selectivity promoter to Fe-based FTS catalysts.

## ■ AUTHOR INFORMATION

### Corresponding Author

\*E-mail: davis@caer.uky.edu.

## ■ ACKNOWLEDGMENT

The work carried out at the CAER was supported in part by funding from a seed grant from the Kentucky Governor's Office of Energy Policy (Solicitation 08-GOEP-02), as well as the Commonwealth of Kentucky. Argonne's research was supported in part by the U.S. Department of Energy (DOE), Office of Fossil Energy, National Energy Technology Laboratory (NETL). The use of the Advanced Photon Source was supported by the U.S. Department of Energy, Office of Science, Office of Basic Energy Sciences, under Contract DE-AC02-06CH11357. MRCAT operations are supported by the Department of Energy and the MRCAT member institutions.

## ■ REFERENCES

- Jacobs, G.; Sarkar, A.; Davis, B. H.; Cronauer, D. C.; Kropf, A. J.; Marshall, C. L. Temperature Programmed EXAFS/XANES Characterization of the Impact of Cu and Alkali Promoters to Iron-Based Catalysts on the Carbide Formation Rate. In *Advances in Fischer-Tropsch Synthesis, Catalysts and Catalysis*; CRC Press, Taylor & Francis Group: Boca Raton, FL, 2010, pp 119–146, Chapter 7.
- Ribeiro, M. C.; Jacobs, G.; Davis, B. H.; Cronauer, D. C.; Kropf, A. J.; Marshall, C. L. Fischer-Tropsch synthesis: An in-situ EXAFS/XANES study of the influence of Group I alkaline promoters on the structure of carburized iron catalysts. *J. Phys. Chem. C* **2010**, *114*, 7895–7903.
- Kolbel, H.; Tillmetz, K. D. Hydrocarbons and oxygen-containing compounds and catalysts therefore. US Patent 19791204, 1979.
- Lide, D. R. *CRC Handbook of Chemistry & Physics*, 90<sup>th</sup> ed.; CRC Press: Boca Raton, FL, 2009–2010.
- van Dijk, W. L.; Niemantsverdriet, J. W.; van der Kraan, A. M.; van der Baan, H. S. Effects of manganese oxide and sulfate on the olefin selectivity of iron catalysts in the Fischer-Tropsch reaction. *Appl. Catal.* **1982**, *2*, 273–288.
- Das, C. K.; Das, N. S.; Choudhury, D. P.; Ravichandran, G.; Chakrabarty, D. K. Hydrogenation of carbon monoxide on unsupported Fe–Mn–K catalysts for the synthesis of lower alkenes: promoter effect of manganese. *Appl. Catal. A: Gen.* **1994**, *111*, 119–132.
- Maiti, G. C.; Malessa, R.; Baerns, M. Iron/manganese oxide catalysts for Fischer-Tropsch synthesis. Part I. Structural and textural changes by calcination, reduction and synthesis. *Appl. Catal.* **1983**, *5*, 151–170.
- Maiti, G. C.; Malessa, R.; Löchner, U.; Papp, H.; Baerns, M. Iron/manganese oxide catalysts for Fischer-Tropsch synthesis. Part II: Crystal phase composition, activity and selectivity. *Appl. Catal.* **1985**, *16*, 215–225.
- Krishnakutty, N.; Mulay, L. N.; Vannice, M. A. Magnetic characterization of carbon-supported iron, iron-manganese, potassium-iron, and potassium-iron-manganese catalysts prepared from carbonyl clusters. *J. Phys. Chem.* **1992**, *96*, 9944–9951.
- Kolk, B.; Albers, A.; Leith, I. R.; Howden, M. G. Mössbauer and x-ray studies of the structure of iron-manganese oxide catalyst precursors. *Appl. Catal.* **1988**, *37*, 57–74.
- Kreitman, K. M.; Baerns, M.; Butt, J. B. Manganese-oxide-supported iron Fischer-Tropsch synthesis catalysts: Physical and catalytic characterization. *J. Catal.* **1987**, *105*, 319–334.
- Jensen, K. B.; Massoth, F. E. Studies on iron-manganese oxide carbon monoxide catalysts. II. Carburization and catalytic activity. *J. Catal.* **1985**, *92*, 109–118.
- Hughes, I. S. C.; Newman, J. O. H.; Bond, G. C. The characterization of unsupported iron and manganese-promoted iron catalysts by X-ray photoelectron spectroscopy and temperature-programmed reduction. *Appl. Catal.* **1987**, *30*, 303–311.
- Grzybek, T.; Papp, H.; Baerns, M. Iron/manganese oxide catalysts for Fischer-Tropsch synthesis. Part V. XPS surface characterization of calcined and reduced samples. *Appl. Catal.* **1987**, *29*, 335–350.
- Copperthwaite, R. G.; Hack, H.; Hutchings, G. J. X-ray photoelectron spectroscopic evidence for iron enrichment on doped manganese oxide surfaces. *Surf. Sci.* **1985**, *164*, L827–L830.
- Soong, Y.; Rao, V. U. S.; Gormley, R. J. Temperature-programmed desorption study on manganese-iron catalysts. *Appl. Catal.* **1991**, *78*, 97–108.
- Campos, A.; Lohitharn, N.; Roy, A.; Lotero, E.; Goodwin, J. G., Jr.; Spivey, J. An activity and XANES study of Mn-promoted, Fe-based Fischer-Tropsch catalysts. *Appl. Catal. A: Gen.* **2010**, *375*, 12–16.
- Morales, F.; de Groot, F. M. F.; Glatzel, P.; Kleimenov, E.; Bluhm, H.; Hävecker, M.; Knop-Gericke, A.; Weckhuysen, B. M. in situ X-ray Absorption of Co/Mn/TiO<sub>2</sub> Catalysts for Fischer-Tropsch Synthesis. *J. Phys. Chem. B* **2004**, *108*, 16201–16207.
- Morales, F.; Grandjean, D.; Mens, A.; de Groot, F. M. F.; Weckhuysen, B. M. X-ray absorption spectroscopy of Mn/Co/TiO<sub>2</sub> Fischer-Tropsch catalysts: Relationships between preparation method, molecular structure, and catalyst performance. *J. Phys. Chem. B* **2006**, *110*, 8626–8639.
- Milburn, D. R.; Chary, K. V. R.; O'Brien, R. J.; Davis, B. H. Promoted iron Fischer-Tropsch catalysts: Characterization by thermal analysis. *Appl. Catal. A: Gen.* **1996**, *144*, 133–146.

- (21) Deppe, P.; Papp, H.; Rosenberg, M. Mössbauer spectroscopic investigations of iron-manganese-Fischer–Tropsch-catalysts. *Hyperfine Interact.* **1986**, *28*, 903–906.
- (22) Hutchings, G. J.; Boeyens, J. C. A. Effect of iron manganese oxide solid solutions on selectivity for lower hydrocarbons from carbon monoxide hydrogenation. *J. Catal.* **1986**, *100*, 507–511.
- (23) Campos, A.; Lohitharn, N.; Roy, A.; Goodwin, Jr., J. G.; Spivey, J. J. Using *in-situ* Fe and Mn K-edge XANES to study a Mn-promoted Fe/Cu/SiO<sub>2</sub> catalyst during H<sub>2</sub> reduction and during the Fischer–Tropsch synthesis. Abstracts of Papers, 240th ACS National Meeting, Boston, MA, United States, August 22–26, 2010.
- (24) Lohitharn, N.; Goodwin, J. G., Jr.; Lotero, E. Fe-based Fischer–Tropsch synthesis catalysts containing carbide-forming transition metal promoters. *J. Catal.* **2008**, *255*, 104–113.
- (25) Davis, B. H. Fischer–Tropsch Synthesis: Reaction mechanisms for iron catalysts. *Catal. Today* **2009**, *141*, 25–33.
- (26) Ressler, T. WinXAS: A program for x-ray absorption spectroscopy data analysis under MS-Windows. *J. Synch. Rad.* **1998**, *5*, 118–122.
- (27) Teo, B. K. *EXAFS: Basic Principles and Data Analysis, Inorganic Chemistry Concepts 9*; Springer Verlag: Berlin, Heidelberg, New York, 1986.
- (28) Stolzenberg, A. M. *Kirk-Othmer Encyclopedia of Chemical Technology*, 4<sup>th</sup> ed.; Wiley Interscience: New Jersey, 1995 Vol. 14, p 883.
- (29) Yamamoto, T. Assignment of pre-edge peaks in K-edge x-ray absorption spectra of 3d transition metal compounds: electric dipole or quadrupole? *X-ray Spectrometry* **2008**, *37*, 572–584.
- (30) Colombo, U.; Gazzarrini, F.; Lanzavecchia, G. Mechanisms of reduction of iron oxides at temperatures below 400°. *Mater. Sci. Eng.* **1967**, *2*, 125–134.
- (31) Khalid, S. <http://x18b.nsls.bnl.gov/data.htm>.
- (32) Englisch, M.; Lercher, J. A.; Haller, G. L. in: Iwasawa, Y. (Ed.), *X-ray Absorption Fine Structure for Catalysts and Surfaces*; World Scientific Publishing Co. Pte. Ltd.: London, 1996.
- (33) Asensio, M. C.; Kerkar, M.; Woodruff, D. P.; de Carvalho, A. V.; Fernandez, A.; Gonzalez-Elipe, A. R. The growth of thin titanium and titanium oxide films on platinum(111): morphology and oxidation states. *Surf. Sci.* **1992**, *273*, 31–39.
- (34) Jacobs, G.; Das, T. K.; Zhang, Y.; Li, J.; Racollet, G.; Davis, B. H. Fischer–Tropsch synthesis: support, loading and promoter effects on the reducibility of cobalt catalysts. *Appl. Catal. A: Gen.* **2002**, *233*, 263–281.
- (35) de Smit, E.; Weckhuysen, B. M. The renaissance of iron-based Fischer–Tropsch synthesis: On the multifaceted catalyst deactivation behavior. *Chem. Soc. Rev.* **2008**, *37*, 2758–2781.
- (36) Nagakura, S. Study of metallic carbides by electron diffraction. III. Iron carbides. *J. Phys. Soc. Jpn.* **1959**, *14*, 186–195.
- (37) Ravel, B. *Proceedings of the Workshop on EXAFS Analysis Using FEFF and FEFFIT*; Brookhaven National Laboratory: Upton, NY, 2001.
- (38) O'Brien, R. J.; Davis, B. H. Impact of Copper on an Alkali Promoted Iron Fischer–Tropsch Catalyst. *Catal. Lett.* **2004**, *94*, 1–6.
- (39) Luo, M.; Hamdeh, H.; Davis, B. H. Fischer–Tropsch Synthesis: Catalyst activation of low alpha iron catalyst. *Catal. Today* **2009**, *140*, 127–134.
- (40) van der Laan, G. P.; Beenackers, A. A. C. M. Kinetics and selectivity of the Fischer–Tropsch synthesis: a literature review. *Catal. Rev.: Sci. Eng.* **1999**, *41*, 255–318.